Received: 22 February 2020 | Revised: 26 May 2020 | Accepted: 23 June 2020

DOI: 10.1002/app.49655

ARTICLE

Applied Polymer SCIENCE WILEY

Spatially resolved indiffusion behavior of Cu^{2+} and Ni^{2+} in polypropylene

Stefanie Kern[1] | Christine Kern[1] | Mark Melvin Pradja[1] | Rolf-Alexander Düring[2,3] | Marcus Rohnke[1,3]

[1]Institute of Physical Chemistry, Justus Liebig University Giessen, Giessen, Germany

[2]Institute of Soil Science and Soil Conservation, Research Center for Biosystems, Land Use and Nutrition, Justus Liebig University Giessen, Giessen, Germany

[3]Center for Materials Research, Justus Liebig University Giessen, Giessen, Germany

Correspondence
Marcus Rohnke, Institute of Physical Chemistry, Justus Liebig University Giessen, Heinrich-Buff-Ring 17, 35392 Giessen, Germany.
Email: marcus.rohnke@phys.chemie.uni-giessen.de

Abstract

Microplastics and their effects on the environment and food chain have become increasingly important in recent years. These polymer particles, which are only few millimeters in size or smaller, accumulate in the environment and can enter the human food chain via animals that ingest them. Moreover, they can accumulate impurities such as heavy metals. Therefore, this study focuses on the indiffusion behavior of metal ions into semicrystalline polypropylene (PP) applying time-of-flight secondary ion mass spectrometry (ToF-SIMS) at cryo-conditions. Diffusion coefficients of Cu^{2+} and Ni^{2+} in PP are determined by classical SIMS depth profiling in frozen state ($T < -130°C$) and subsequent data analysis according to Fick's second law of diffusion. The results show that diffusion of Cu^{2+} ions in dry PP ($D_{PP,Cu} = [2.21 \pm 0.15] \cdot 10^{-12}$ cm^2/s) is faster compared to Ni^{2+} ion diffusion of dry PP ($D_{PP,Ni} = [4.43 \pm 0.55] \cdot 10^{-13}$ cm^2/s). Interestingly, the diffusion of Cu^{2+} ions in water-saturated PP ($D_{PP,H2O,Cu} = [1.91 \pm 0.28] \cdot 10^{-13}$ cm^2/s) is slower compared to Cu^{2+} ion diffusion in dry PP. Furthermore, high-lateral resolution ToF-SIMS analysis shows that metal ions only diffuse in certain areas of PP, which are most likely amorphous.

KEYWORDS

kinetics, surfaces and interfaces, thermoplastics

1 | INTRODUCTION

Due to the increasing use of plastics and microplastics (size <5 mm) in everyday life, there is an accumulation of microplastics in the aquatic and terrestrial ecosystem.[1,2] Plastics are mostly synthetic organic polymers, comprised of monomeric repeat units.[3] The term polymer refers to the composition, whereas the term plastic refers mainly to the properties of the material.[4] Global production of plastics was over 348 million tons in 2018.[5] The polymers most commonly produced as plastics are polypropylene (PP), polyethylene (high and low density), polystyrene, polyethylene terephthalate, polyurethane, and polyvinylchloride.[6]

Microplastics in the environment can arise from different sources. Secondary microplastic particles result from slow fragmentation of larger plastic particles in the environment for example, through abrasion of car tires, fragmentation or weathering by UV radiation, wind or waves. In addition, microplastics can also be so-called

primary particles, which are used, for example, in body care products, such as rubbing agents in cosmetics, shower gels or toothpaste, laser sinter powder for 3D printing, or plastic granulates in industry.[6]

Accumulation of polymer particles and microplastic fragments in the environment are not only of eco-toxicological interest, but also with regard to possible negative effects on human health.[7] Polymer particles can take up, accumulate and release various environmental organic toxicants, such as dichlorodiphenyltrichloroethane (DDT), polychlorinated biphenyls (PCBs), and polycyclic aromatic hydrocarbons (PAH).[8,9] In addition, heavy metals like lead, nickel, cobalt, or cadmium as well as other metals (e.g., copper, alkali metals, zinc) can also accumulate in plastic particles.[10] The addition of additives, such as plasticizers, fillers, antioxidants, flame retardants, and colorants to polymers during their manufacturing is another source of chemicals with potential human and environmental health risks.[11] Therefore, hazardous contaminants and chemicals can derive from the polymer's monomeric building block (e.g., bisphenol A in polycarbonate), from polymer additives, from accumulation of environmental pollutants or from a combination of all.[2,11,12]

Hong et al showed in 2017, that although data on microplastics in the environment have increased recently, there is still limited information on chemicals, toxicants, and pollutants associated with microplastics.[13] Information on metals and plastic additives is even more scarce. The most studied chemicals associated with microplastics are organic pollutants, such as PCBs, PAHs, and DDTs.[13,14] Analytical methods applied to the chemical analysis of microplastics often include a series of sample preparation steps, such as extraction, purification, and instrumental analysis. For quantitative and qualitative analysis of plastic particles, chemicals and pollutants, chromatographic techniques (e.g., gas chromatography) are frequently used in combination with mass spectrometry. However, those methods provide only insight in the integral amount of chemicals of the plastic fragments.[13] For analysis of the transport of inorganic and organic chemicals either from water/environment to microplastics or the other way around, the individual chemical and physical processes of the transport kinetics have to be investigated.[14]

It is believed that the rate-limiting step of the absorption of organic molecules and metals by plastics is often diffusion in the plastic phase.[14] Thus, our present study aims at providing first insight into metal ion diffusion into polymers and their interaction. The semicrystalline polymer PP was chosen as model polymer, because of its relevance to the environment and PP being one of the most produced plastic polymers today.[15,16] We selected copper ions for this study, because copper is not only an essential metal, but also a common contaminant of ecosystems. In addition, copper is also toxic to several microalgae and used in antimicrobial applications.[17,18] Nickel ions were chosen as heavy metal ion species. Nickel is widely used in industry for example, in power plants, nickel-cadmium batteries, and in the plastic industry. Nickel-induced toxicities include genotoxicity, carcinogenicity, and immunotoxicity.[19,20]

The general aim of this study is the spatially resolved investigation of metal ion diffusion in PP. Therefore, a time-of-flight secondary ion mass spectrometry (ToF-SIMS) based cryo-approach should be established. ToF-SIMS provides locally resolved depth profiles and also full three-dimensional analysis data by applying, in addition to the analysis beam, a sputter ion beam, which removes the sample layer by layer.[21] Afterward, those depth profiles can be used for calculations of diffusion coefficients of metal ions in PP. This is to our best knowledge the first time, that such an approach is used in this field of research.

2 | EXPERIMENTAL

2.1 | PP and metal solutions

PP homopolymer was purchased from Goodfellow (425–485-97, Hamburg, Germany) as a biaxially orientated 150×150 mm^2 sheet of 1.0 mm thickness and a density of 0.9 g/cm^3. This PP can absorb water until an equilibrium state of 0.03%. Permeability to water at 25°C is 16×10^{-13} (cm^3 cm)/(cm^2 s Pa). Although the tacticity of PP was not determined for the sold batch, Goodfellow points out that their commercial PP is predominantly isotactic (all data are taken from the data sheet). For analysis, PP sheet was cut into small pieces of approximately 1.0×1.0 cm^2. Solutions of $Cu(NO_3)_2 \cdot 3\ H_2O$ and $Ni(NO_3)_2 \cdot 6\ H_2O$ were freshly prepared for diffusion experiments with concentrations of 1 mol/L. The high metal salt concentration was chosen to obtain good signal to noise ratios for the subsequent mass spectrometric analyses.

2.2 | Surface roughness determination with AFM

Surface of PP sheet was characterized using a high performance atomic force microscope MultiMode 8 (Bruker, Germany). PP sheets were fixed to the sample stage with double-sided stick tape. Images were obtained in the general image mode "ScanAsyst" which is based on the "PeakForce Tapping" mode by Bruker. Height images were

collected across a 20 × 20 μm^2 area. Images were afterward processed using the Gwyddion software 2.53 (http://www.gwyddion.net)[22]. Surface roughness was quantified by the root mean square (RMS) roughness. RMS, maximum peak height (*Sp*), maximum pit depth (*Sv*), and maximum height (*Sz*) of the scanned surfaces were calculated and profiles were recorded with Gwyddion 2.53.

2.3 | Surface characterization of PP with ToF-SIMS

ToF-SIMS measurements were carried out in the positive ion mode with a TOF.SIMS 5 machine (IONTOF GmbH, Muenster, Germany) equipped with a bismuth cluster primary ion source (25 keV) and Cs, O_2, and Ar_x sputter guns. For high-resolution surface images, the fast imaging (burst alignment) mode was applied. For each measurement 25 keV Bi_3^+ ions were used as analysis species. The pattern was 512 × 512 pixel. This led to pixel resolutions of 585 nm/pixel for an area of 300 × 300 μm^2, 195 nm/pixel for an area of 100 × 100 μm^2, and 97 nm/pixel for an area of 50 × 50 μm^2. Other analyses parameters were a cycle time of 80 μs, one shot/frame/pixel and one frames/patch. Primary ion current was about 0.06–0.08 pA. Charge compensation was done with a low-energy electron flood gun. Internal mass calibration was performed using CH_2^+, CH_3^+, $C_2H_2^+$, $C_2H_3^+$, $C_3H_5^+$, and $C_4H_7^+$ mass signals in positive ion mode.

Data analysis of ToF-SIMS measurements was carried out with the Surface Lab Software version 7.0 (IONTOF GmbH). Regions-of-interest (ROIs) were manually delineated and ToF-SIMS image dataset was analyzed by applying principal component analysis (PCA). The SurfaceLab software employs image PCA for identification relationships between the lateral distribution of secondary ions in ion images and highlights the largest differences. After selecting the appropriate mass channels, a series of PCA images was generated by the PCA data processing, calculated with the SurfaceLab software. For each principle component (PC), one image was formed which arises from the combined analysis of the chosen mass channels. The PCs were ordered by the explained variance in the data set.

2.4 | Determination of Me^{2+} uptake by inductively coupled plasma optical emission spectroscopy

Inductively coupled plasma optical emission spectroscopy (ICP-OES) of the used metal solutions was carried out on a Varian 720 ES. To obtain quantitative values for the metal absorption, PP disks of 1 × 1 cm^2 were stored for 1 week in 10 ml of the metal ion solution. The metals concentration was measured at the beginning and after 1 week by ICP-OES (emission lines 222.486 and 227.021 nm for Ni^{2+}; 324.754 and 327.395 nm for Cu^{2+}). The experiment was carried out five times for each metal. The starting concentration was 20 mg/L for Nickel(II) nitrate hexahydrate and Copper(II) nitrate trihydrate.

2.5 | Diffusion experiments

For determination of diffusion coefficients of Cu^{2+} and Ni^{2+}, 1 mol/L metal salt solutions were dropped onto PP surface. Residence time was 1 hr for all metal ion solutions on dry PP samples (Figure 3a). In a second approach, diffusion of metal ions in wet PP was determined. Therefore, PP samples were stored in demineralised water for at least 3 days to ensure water absorption equilibrium. Thereafter, metal solutions were again dropped onto PP surface. Residence time for Ni^{2+}-solution was 1 hr (dry PP) or 1.5 hr (wetted PP). In order to obtain a time series of copper diffusion, residence time of Cu^{2+}-solution on wet PP samples was 1 hr, 2 hr and 4 days. In all cases, diffusion was stopped by cooling samples down below 0°C with liquid nitrogen inside the load lock chamber of the ToF-SIMS instrument. After reaching temperature lower than 0°C, evacuation to vacuum was started and the sample was transferred to the analysis chamber of the ToF-SIMS instrument, where samples were further cooled with liquid nitrogen below −130°C during the whole measurements. The rapid cooling below 0°C was achieved in all cases in less than 1 min.

2.6 | Depth profiles and surface characterization with ToF-SIMS

For ToF-SIMS depth profiling (see Figure 3b,c), a standard IONTOF heating/cooling sample holder was used. For all reported measurements, sample temperature was kept below −130°C in the analysis chamber. Depth profiling was performed in noninterlaced mode. Sample surface was in each case analyzed in an area of 50 × 50 μm^2 with 25 keV Bi_3^+ ions as analysis species. The primary ion gun was operated in the spectrometry mode with 150 μs cycle time, 128 × 128 pixel with three shot/frame/pixel and five frames/patch. The ion beam current was about 0.06–0.08 pA. The obtained mass resolution $m/\Delta m$ at FWHM was for all measurements better than 3,500 for the $C_5H_9^+$ mass signal. To improve the focus of the primary ion beam (and hence the lateral resolution), pulse width of Bi_3^+ (25 keV) ion pulse was reduced to 6 ns.

After each analysis scan, sample surface was sputtered for 1 s with 10 keV Ar_{1500}^+ ions for depth profiling. Sputter pause for charge compensation was 5 s. Sputter beam area was 250 × 250 μm^2 and centred on the analysis area to avoid crater-wall effects. The sputter current was between 9.5 and 12.5 pA. Charge compensation was done with a low-energy electron flood gun (20 eV). Internal mass calibration was carried out by using CH_2^+, CH_3^+, $C_2H_2^+$, $C_2H_3^+$, $C_3H_5^+$, and $C_4H_7^+$ mass signals in positive ion mode. Data analysis of the ToF-SIMS measurements was done with the Surface Lab Software version 7.0 (IONTOF GmbH). ROIs were manually delineated and depth profiles within the defined regions were extracted.

After ToF-SIMS depth profiling, the depth of sputter craters was measured with a confocal microscope PLu neox 3D (Sensofar, Terrassa, Spain) to calibrate the sputter time axis and to calculate the erosion rate. We assumed a constant sputtering rate for the calibration of the depth profiles.

2.7 | Imaging of Cu^{2+} diffusion

For high-resolution imaging analysis of copper ion diffusion into PP, PP surface was cleaned with 5 keV Ar_{1500}^+ sputter beam before applying imaging analysis in delayed extraction mode. As analysis species, 25 keV Bi_3^+ ions species were used. The delay time of 55 ns was adjusted according to an optimized mass signal intensity and mass resolution. Parameters for the analysis in Figure 7 were the following: cycle time 100 μs, rastered in sawtooth mode, three frames per patch, three shots per frame per pixel, 20 scans. The pattern was 512 × 512 pixel. This led to a pixel resolution of 293 nm/pixel for an area of 150 × 150 μm^2. Primary ion current was 0.103 pA. Charge compensation was done with a low-energy electron flood gun (20 eV). Internal mass calibration was performed by using $C_2H_3^+$, $C_3H_5^+$, $C_4H_7^+$, $C_4H_9^+$, and $C_5H_9^+$ mass signals in positive mode.

Data analysis of all ToF-SIMS measurements was done with the Surface Lab Software version 7.0 (IONTOF GmbH, Münster, Germany).

2.8 | Statistical analysis

Normal distribution of experimental data was tested using the Shapiro–Wilk test. Differences in diffusion coefficients were analyzed using two-way analysis of variance test accompanied by two-sample *t*-test in case of normal distribution. The Mann–Whitney *U* test was used after ascertaining a non-normal distribution. Diffusion coefficients, RMS, *Sp*, *Sv*, and *Sz* are reported as means ± *SEM*. A value of $p < .05$ was regarded as statistically significant. Statistical analyses were performed using Origin v9.3 (OriginLab Corporation, Northampton, MA).

3 | RESULTS

This study provides insight into metal ion indiffusion into commercially available PP at room temperature. PP is a semicrystalline isotactic polymer with both, crystalline and amorphous regions. Therefore, in order to investigate crystallinity and morphology of the surface of PP samples, AFM, and ToF-SIMS surface analyses were conducted first.

3.1 | Characterization of PP surface—AFM

AFM is often the first choice method for the study of the roughness of polymer surfaces.[23] Here, we used the ScanAsyst mode by Bruker for analyzing the PP surface morphology. In this mode, the cantilever response is decoupled from resonance dynamics, which allows automatic adjustment of all important scanning parameters.[24] AFM images of PP surface are presented in Figure 1. The corresponding surface roughness was quantified by the RMS roughness. Topographical images of the PP surface were obtained at three different locations. Overall, average RMS of the measured PP surfaces ($n = 3$) was 30.4 ± 2.5 nm (Figure 1). Average maximum peak height (*Sp*) was 109.4 ± 12.4 nm, average maximum pit depth (*Sv*) was 96.0 ± 9.2 nm and finally the average maximum height was 205.4 ± 21.4 nm. The surface roughness was negligible in our further ToF-SIMS studies due to the low measured values in comparison to the sputter depth of several micrometers. Unfortunately, it was not possible to obtain atomic (molecular) resolution to make a statement about different orientations of the polymer molecules and crystal structure.

3.2 | PP surface characterization with ToF-SIMS

High-lateral-resolution surface images of PP were recorded with ToF-SIMS applying fast imaging mode in order to investigate surface areas in detail. For distinction of different areas, a PCA of the obtained imaging data was carried out.

PCA analysis of 100 × 100 μm^2 positive secondary ion image (see Figure 2) results in the identification of two different areas on the PP surface. Positive loadings refer to mass fragments with relatively high signal intensities in the mass spectra of the corresponding image score.

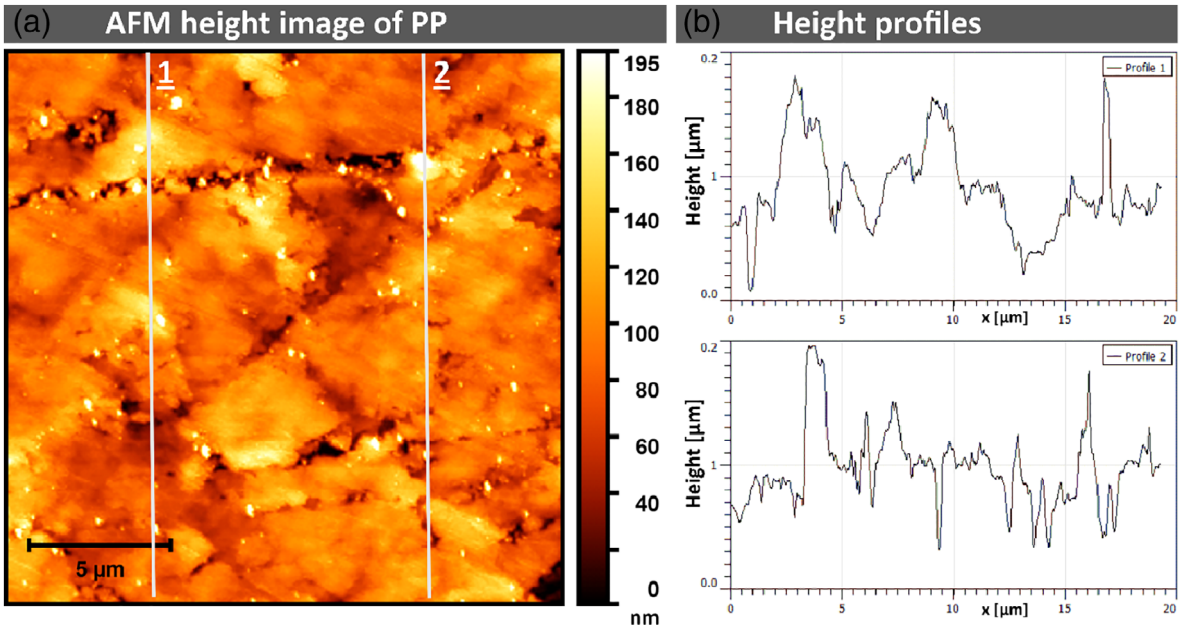

FIGURE 1 Surface roughness and topography of polypropylene (PP) characterized by AFM. (a) AFM height image shows surface topography of PP (scale bar = 5 µm). White lines 1 and 2 identify the location of the corresponding height profiles shown in (b). Surface roughness was quantified by the root mean square (RMS) roughness. Mean RMS is 30.3 ± 2.5 nm ($n = 3$) [Color figure can be viewed at wileyonlinelibrary.com]

Negative loadings refer to mass fragments that show an anticorrelation to the image score. Therefore, these mass fragments are responsible for the discrimination of different areas of PP surface. Image scores with factor loadings of PC1 (93.48% of the total variance) are presented in Figure 2a,d. Image score for PC1 shows strong positive loading fragments found for masses, such as $C_3H_5^+$ (*m/z* 40.94), $C_3H_7^+$ (*m/z* 42.98), $C_4H_7^+$ (*m/z* 55.02), $C_4H_9^+$ (*m/z* 56.98), and $C_5H_9^+$ (*m/z* 68.97).

In comparison, image scores for PC2 (3.64% of the total variance) (Figure 2c) show same pattern as ROI 2, with strong positive loading found for $C_3H_3^+$ (*m/z* 38.94) (Figure 2e. Negative loadings for PC2 include masses, such as $C_3H_7^+$ (*m/z* 42.98), $C_4H_7^+$ (*m/z* 55.02), $C_4H_9^+$ (*m/z* 56.98), and $C_5H_9^+$ (*m/z* 68.97). These mass fragments, which are the same mass fragments correlated with image score for PC1, are anticorrelated with PC2 image score.

3.3 | Investigation of metal ion diffusion in PP

After surface characterization, metal ion diffusion experiments were conducted. An imaging mass spectrometry approach was used for experimental determination of Ni^{2+} and Cu^{2+} diffusion coefficients in commercially available PP sheets. A schematic workflow is depicted in Figure 3. 1 M aqueous metal ion solutions were dropped onto pieces of PP. After a certain residence time, metal ion solutions were removed from samples and further metal diffusion was stopped by cooling PP samples inside the ToF-SIMS intro chamber with liquid nitrogen (Figure 3a). Samples were maintained cool during analysis in order to ensure that no further diffusion took place. ToF-SIMS depth profiling was used for resolving metal ion distribution in PP (Figure 3b). Briefly, so-called secondary ions are produced by a pulsed primary ion beam and are analyzed in a time-of-flight mass analyzer. Alternating to analysis scans the sample is removed layer by layer by a sputter ion beam to obtain 3D mass maps and diffusion profiles (Figure 3c). Despite of their original chemical nature, secondary ions from ToF-SIMS measurements are mostly single charged. Hence, for this work it was assumed that the detected Ni^+ and Cu^+ ions originate from Ni^{2+} and Cu^{2+} precursor ions.

Depth profiling capabilities of the used argon cluster source (Ar_{1500}^+) provides detailed information about the diffusion of metal ions into PP. Diffusion coefficients of Ni^{2+} and Cu^{2+} in PP were calculated from obtained ToF-SIMS data of depth profiles. For calculation of the diffusion coefficients, sputter rates were determined in the first step. Thereby, sputter craters with flat grounds are mandatory for evaluation of precise diffusion coefficients. In order to define an exact sputtering rate, exact knowledge of the crater depth in the examined material is required in addition to sputtering time. Commercial PP samples were sputtered with 10 keV Ar-clusters

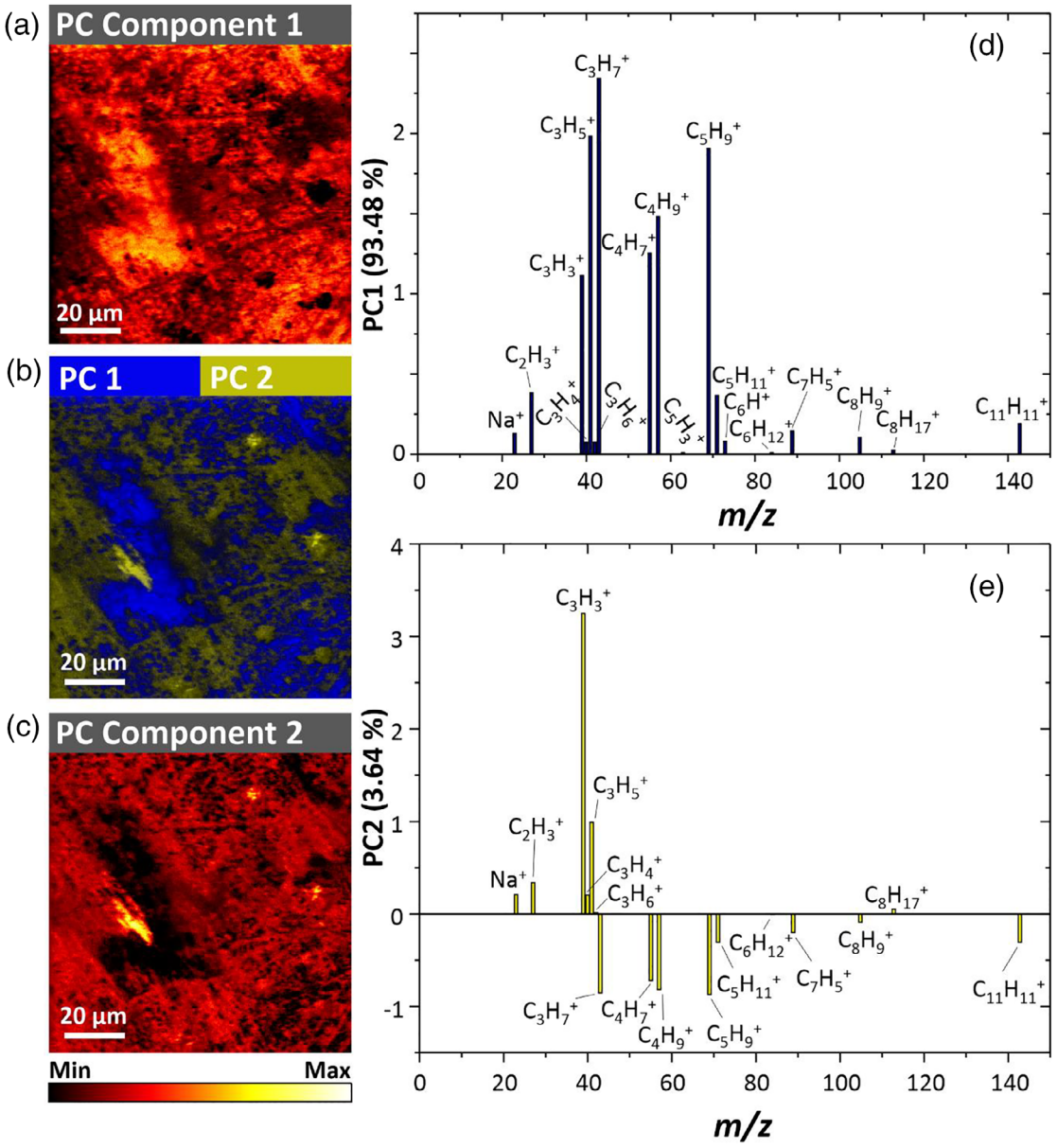

FIGURE 2 Principal component analysis (PCA) scores images and loadings plots of positive ion time-of-flight secondary ion mass spectrometry (ToF-SIMS) spectra of the polypropylene surface. (a), (d) PCA score image with corresponding loading plot for PC1 (93.48%). (c), (e) PCA score image with corresponding loading plot for PC2 (3.64%). (b) Overlay image of PC1 and PC2 [Color figure can be viewed at wileyonlinelibrary.com]

(Ar_{1500}^+) at different sputter times and resulting depths of sputter craters were afterward analyzed with confocal microscopy (Figure S1, supporting information). With the assumption that the sputter rate was constant throughout experiments, sputter rate for 10 keV Ar-clusters (Ar_{1500}^+) on PP was determined as in average 83.75 nm/s. This value was used for all following ToF-SIMS depth profiles for calibration of the sputter time axis.

Data evaluation was carried out by fitting a suitable mathematical solution of Fick's second law of diffusion to the experimentally obtained diffusion profiles. Fick's second law can be applied when the concentration of the penetrant changes at a particular location of the system with respect to time. According to Fick's second law, the basic equation of mass uptake by a polymer film or sheet is given by Equation (1), where n is related to the type of diffusion mechanism and k is a constant which depends on diffusion coefficient D and film thickness.[26–28] M_t is the amount of a substance diffusing into the polymer as function of time t with M_∞ as the total amount of the substance after reaching thermodynamic equilibrium.[26,29]

$$\frac{M_t}{M_\infty} = kt^n. \quad (1)$$

Fickian diffusion in polymer systems is observed when the temperature is well above the glass transition temperature of the polymer T_g. In this case, it is expected that M_t/M_∞ is proportional to the square-root of time, that is, $n = 0.5$.[26] Our diffusion experiments were conducted at room temperature, which is well above the glass transition temperature of PP (isotactic PP: $T_g = -18°C$).[30] Hence, Fick's second law was applied for this work. For solving Fick's second law (Equation (2)), diffusion from an exhaustless source into semi-infinite space was assumed as boundary condition and Equation (3) is a suitable solution of the differential equation.[26]

$$\frac{\partial c}{\partial t} = \frac{\partial}{\partial x}\left[D\frac{\partial c}{\partial x}\right]. \quad (2)$$

A mathematical fit (Equation (3)) was carried out with the obtained ion signal intensities from ToF-SIMS depth profiles, due to the proportionality between species concentration and secondary ion intensity in ToF-SIMS.[31]

$$c(x) = c_{bg} + c_0 \cdot \left(1 - \mathrm{erf}\frac{x - x_0}{2\sqrt{Dt}}\right). \quad (3)$$

In this fit, c_{bg} is the background concentration of metal ions (Cu^{2+} or Ni^{2+}); c_0 is the concentration of the infinite source; x is the depth; x_0 is the starting point of the diffusion profile; D is the diffusion coefficient and t the diffusion time.[31]

The diffusion profiles for each metal ion species were plotted after summing up the mass spectrometric data of each analysis layer from ToF-SIMS depth profiles. Thus, diffusion profiles show ion intensity versus depth (Figures 4 and 5). Due to possible contamination of the sample surface and dotation effects, which can lead to an unsteady matrix with non-reliable secondary ion data, the first measured data points of diffusion profiles were not considered for the fitting process.[31]

To validate the experimental approach for the investigation of metal ion diffusion into PP by ToF-SIMS, a time-dependent experimental series was conducted to confirm whether the obtained diffusion coefficient keeps constant. For this time series, copper diffusion into water-saturated PP was chosen. The experiment was carried out at a total of four different residence times. ToF-SIMS images showed that Cu^{2+} ions only diffused into certain areas (ROIs) of the polymer (Figure 4b). Thus, 3–4 ROIs were selected for each time point and diffusion coefficient of Cu^{2+} ions were determined (Table 1). Overall, average value of Cu^{2+} diffusion coefficient in wetted PP was $D_{PP,H2O,Cu} = (1.91 \pm 0.28)\cdot 10^{-13}$ cm^2/s. Within the error span, no time dependency of the diffusion coefficient was observed. Therefore, we state that our chosen experimental approach is appropriate for the diffusion study.

3.4 | Diffusion of Cu^{2+} ions in dry and water-saturated PP

Diffusion coefficients of copper ions in dry and water-saturated PP were determined. For both studies, diffusion in dry and wetted PP, ToF-SIMS images showed that distribution of copper ions was limited to certain areas of the polymer with an approximate size of 10–20 µm (Figure 4,

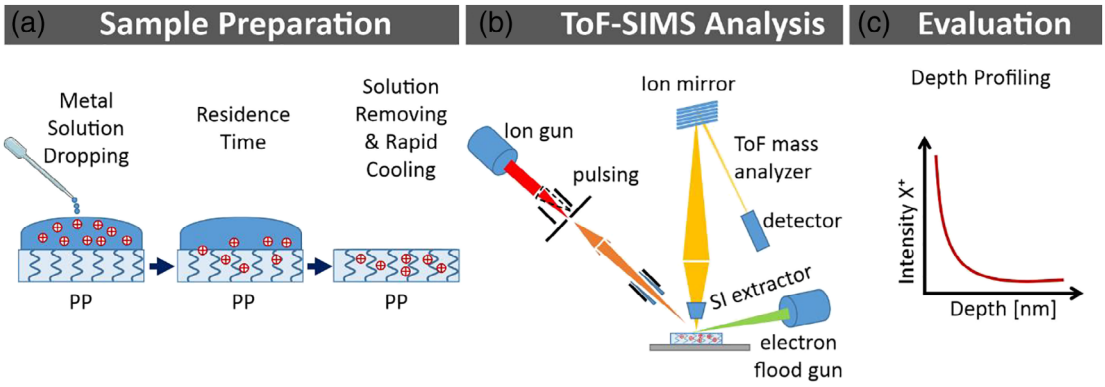

FIGURE 3 Study design of metal ion diffusion experiments with time-of-flight secondary ion mass spectrometry (ToF-SIMS). (a) Metal ion solution was dropped onto polypropylene (PP) surface. After a certain residence time, solution was removed, and sample was rapidly cooled down to stop further diffusion of metal ions into the polymer. (b) Schematic depiction of important internal components of a ToF-SIMS instrument [25]. During the whole analysis time, samples were cooled below −130°C. (c) Schematic example of a depth profile obtained by ToF-SIMS measurement. From this kind of profiles, diffusion coefficients D of metal ions were calculated [Color figure can be viewed at wileyonlinelibrary.com]

Left and Middle). Hence, only those ROIs were used for determination of metal ion diffusion coefficients.

For determination of the Cu^{2+} diffusion coefficient in dry PP, three samples with 4–5 ROIs per sample were measured ($n = 14$). In water-saturated PP, four samples with 3–4 ROIs per sample were evaluated ($n = 15$). Overall, an average diffusion coefficient of $D_{PP,Cu} = (2.21 \pm 0.15) \cdot 10^{-12}$ cm^2/s was obtained for Cu^{2+} diffusion into dry PP samples. Interestingly, average diffusion coefficient for Cu^{2+} diffusion into water-saturated PP samples was lower by one order of magnitude, $D_{PP,H2O,Cu} = (1.91 \pm 0.28) \cdot 10^{-13}$ cm^2/s. Mann–Whitney U test showed a significantly difference ($p = 2.58 \times 10^{-8}$) between Cu^{2+} diffusion in dry and water-saturated PP (Table 2, Figure 6).

3.5 | Diffusion of Ni^{2+} ions in PP

Besides copper diffusion, diffusion of nickel ions in dry and water-saturated PP was investigated. Nickel ions showed the same behavior as copper ions (Figure 4) and only diffused into certain areas of PP (Figure 5). Those regions had a size of approximately 10–20 µm in diameter. Average diffusion coefficients for Ni^{2+} revealed significant differences between dry and water-saturated PP after statistical evaluation (Mann–Whitney U test, $p = 1.603 \cdot 10^{-4}$). Diffusion coefficients of Ni^{2+} ions are $D_{PP,Ni} = (4.43 \pm 0.55) \cdot 10^{-13}$ cm^2/s in dry PP and $D_{PP,H2O,Ni} = (1.45 \pm 0.33) \cdot 10^{-13}$ cm^2/s in water-saturated PP (Table 2, Figure 6).

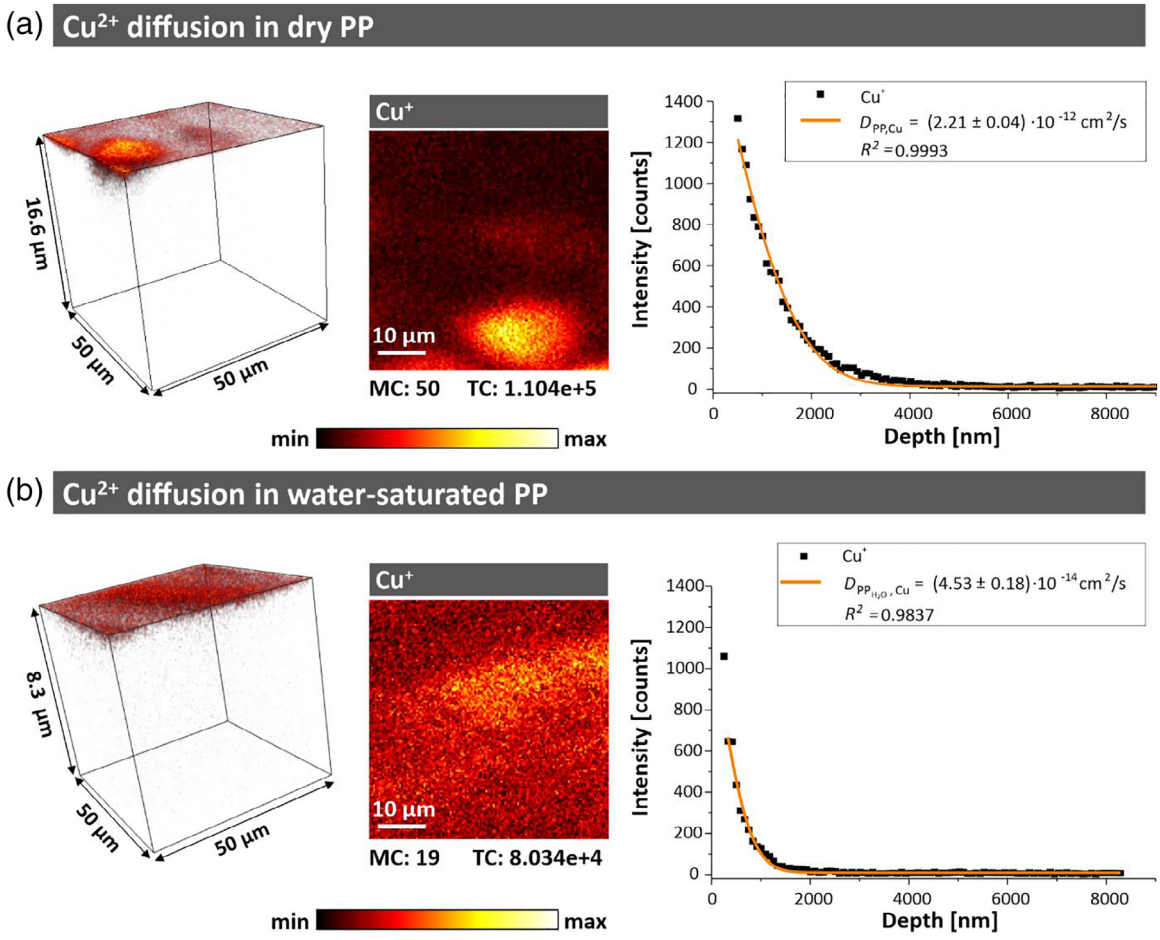

FIGURE 4 Diffusion behavior of Cu^{2+} in dry polypropylene (PP) differed from diffusion behavior in water-saturated PP. (a) Diffusion of Cu^{2+} in PP with a residence time for Cu^{2+} of 1 hr. ToF-SIMS depth profile showed ions diffused approximately 2.5 µm into the polymer. (b) Diffusion of Cu^{2+} in water-saturated PP with a residence time of Cu^{2+} of 1 hr. The depth profile shows that ions diffused approximately 1.5 µm into wetted PP, that is, diffusion was slower compared to dry PP. (a) and (b) Left: 3D mass spectrometry data shows Cu^{2+} diffusion into polymer. Sputtering was done with a 10 keV Ar_{1500}^+ cluster beam; for analysis, Bi_3^+ primary ions were used. Middle: Overview mass images show distribution of the Cu^{2+} signal. Right: Time-of-flight secondary ion mass spectrometry (ToF-SIMS) depth profiles of Cu^{2+} in dry and water-saturated PP. To obtain diffusion coefficients D, diffusion from an exhaustless source into a semi-infinite space was assumed for calculation. The solid lines are the results of the performed fit according to Equation (3) [Color figure can be viewed at wileyonlinelibrary.com]

3.6 | Comparison of diffusion of Cu^{2+} and Ni^{2+} ions in PP

All obtained diffusion coefficients for copper and nickel ions in dry and water-saturated PP are listed in Table 2. Comparison of copper and nickel ion diffusion (Figure 6; *Mann–Whitney U test*, $*p < .05$) reveals a faster diffusion of copper ions into the dry polymer compared to nickel ions (Mann–Whitney U test, $p = 2.58^{-8}$). This trend was also seen in water-saturated PP. Here, however, diffusion of copper ions into PP was not significantly faster than diffusion of nickel ions (Mann–Whitney U test, $p = .055$).

3.7 | Correlation between metal ion diffusion and PP surface areas

ToF-SIMS analyses showed that diffusion of metal ions was limited to certain areas of PP (Figures 4 and 5). In order to investigate these areas of metal ion diffusion in

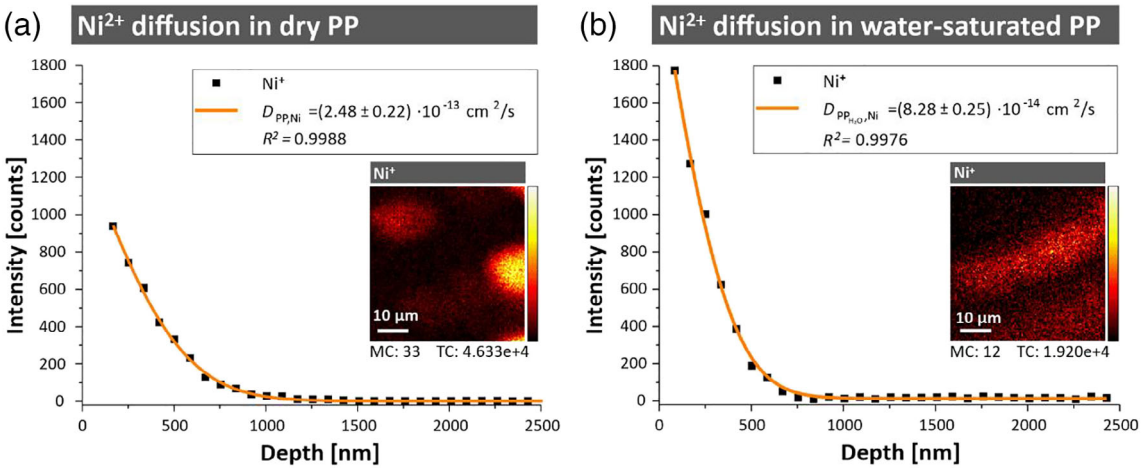

FIGURE 5 Time-of-flight secondary ion mass spectrometry (ToF-SIMS) depth profiles of Ni^{2+} in dry and water-saturated PP. (a) Ni^{2+} ions diffused approximately 1 µm into dry PP after 1 hr residence time. (b) Residence time of Ni^{2+} solution was 1.5 hr. During that time, Ni^{2+} ions diffused about 800 nm into wet PP. (a) and (b) Bi_3^+ primary ions were used for analysis, whereas sputtering was done with a 10 keV Ar_{1500}^+ cluster beam. Overview mass images show the distribution of Ni^{2+} in both dry and water-saturated PP. ToF-SIMS depth profiles of Ni^{2+} in dry and wet PP are shown together with the applied mathematical fit according to Equation (3) [Color figure can be viewed at wileyonlinelibrary.com]

TABLE 1 Time-dependent series of Cu^{2+} diffusion into water-saturated polypropylene PP_{H2O}. For each residence time point, 3–4 ROIs were selected, and diffusion coefficient was determined

Polymer	Metal ion	Residence time [min]	Average diffusion coefficient D [cm^2/s]	*SEM* D [cm^2/s]	ROIs n
PP_{H2O}	Cu^{2+}	60	2.12×10^{-13}	0.84×10^{-13}	4
PP_{H2O}	Cu^{2+}	68	1.18×10^{-13}	0.28×10^{-13}	4
PP_{H2O}	Cu^{2+}	120	1.73×10^{-13}	0.23×10^{-13}	3
PP_{H2O}	Cu^{2+}	5,760	2.56×10^{-13}	0.52×10^{-13}	4
Average value			1.91×10^{-13}	0.28×10^{-13}	15

Abbreviations: PP, polypropylene; ROI, regions-of-interest.

TABLE 2 Average diffusion coefficients for Cu^{2+} and Ni^{2+} in dry and water-saturated PP ± *SEM*

Polymer	Metal ion	Diffusion coefficient D [cm^2/s]	SEM [cm^2/s]	ROIs n
PP_{Dry}	Cu^{2+}	2.21×10^{-12}	0.15×10^{-12}	14
PP_{H2O}	Cu^{2+}	1.91×10^{-13}	0.28×10^{-13}	15
PP_{Dry}	Ni^{2+}	4.43×10^{-13}	0.55×10^{-13}	15
PP_{H2O}	Ni^{2+}	1.45×10^{-13}	0.33×10^{-13}	15

Abbreviations: PP, polypropylene; ROI, regions-of-interest.

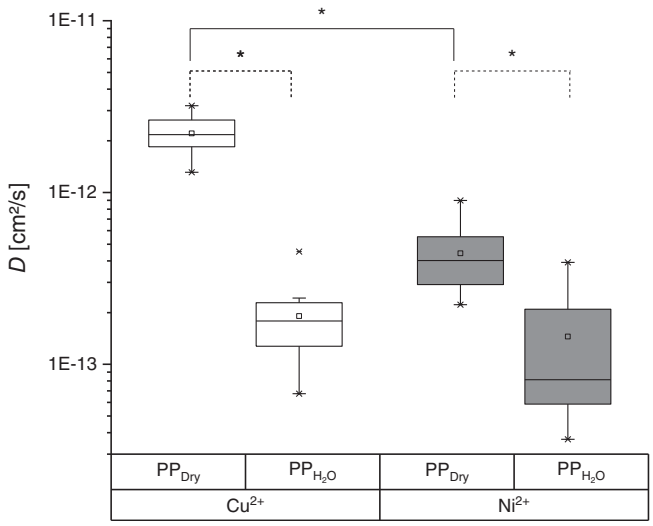

FIGURE 6 Compilation of the diffusion coefficients. Overall, fastest diffusion was Cu^{2+} diffusion into dry PP (n = 14:3 samples, 4–5 ROIs/sample). Cu^{2+} and Ni^{2+} diffusion in dry PP were significantly faster compared to Cu^{2+} diffusion in water-saturated PP (n = 15:4 samples, 3–4 ROIs/sample) ($p = 2.579 \times 10^{-8}$) and Ni^{2+} in water-saturated PP (n = 15:4 samples, 3–4 ROIs/sample) ($p = 1.603 \cdot 10^{-4}$). In addition, diffusion coefficient of Cu^{2+} in dry PP was significantly higher when compared to diffusion coefficient of Ni^{2+} in dry PP (n = 15:4 samples, 3–4 ROIs/sample) ($p = 2.579^{-8}$). Although this pattern was also seen in water-saturated PP, diffusion coefficient of Cu^{2+} was not significantly higher compared to Ni^{2+} (p = .055). (Mann–Whitney U test, *p < .05)

more detail, we applied ToF-SIMS imaging analysis with delayed extraction mode in order to obtain a high lateral resolution. 1 M $Cu(NO_3)_2 \cdot 3\ H_2O$ solution was dropped onto PP surface. After 45 min. residence time, metal ion solution was removed. PP surface was cleaned with 5 keV Ar_{1500}^+ sputter beam before applying high-resolution image analysis (Figure 7).

Together with our PCA results from the first part of this study, a correlation between Cu^{2+} ion indiffusion and different PP surface areas was possible (Figure 7).

The PCA analysis resulted in the identification of two different areas on PP surface, PC component 1 and PC component 2 (Figure 2). As seen in Figure 7, distribution of combined Cu signals is anticorrelated to the distribution of the summed mass fragments of PC component 1 ($C_3H_7^+$ at m/z 43.06, $C_4H_7^+$ at m/z 55.07, $C_4H_9^+$ at m/z 57.07, $C_5H_9^+$ at m/z 69.08, $C_5H_{11}^+$ at m/z 71.06, $C_7H_5^+$ at m/z 88.98, $C_8H_9^+$ at m/z 105.05, and $C_{11}H_{11}^+$ at m/z 143.14). Therefore, Cu^{2+} ion diffusion is slower in PP surface areas identified via PC1.

3.8 | Metal uptake of PP

ToF-SIMS enables the determination of the metal ion diffusion coefficients. Nevertheless, we obtained no value for the absolute quantity of accumulated metal in PP.

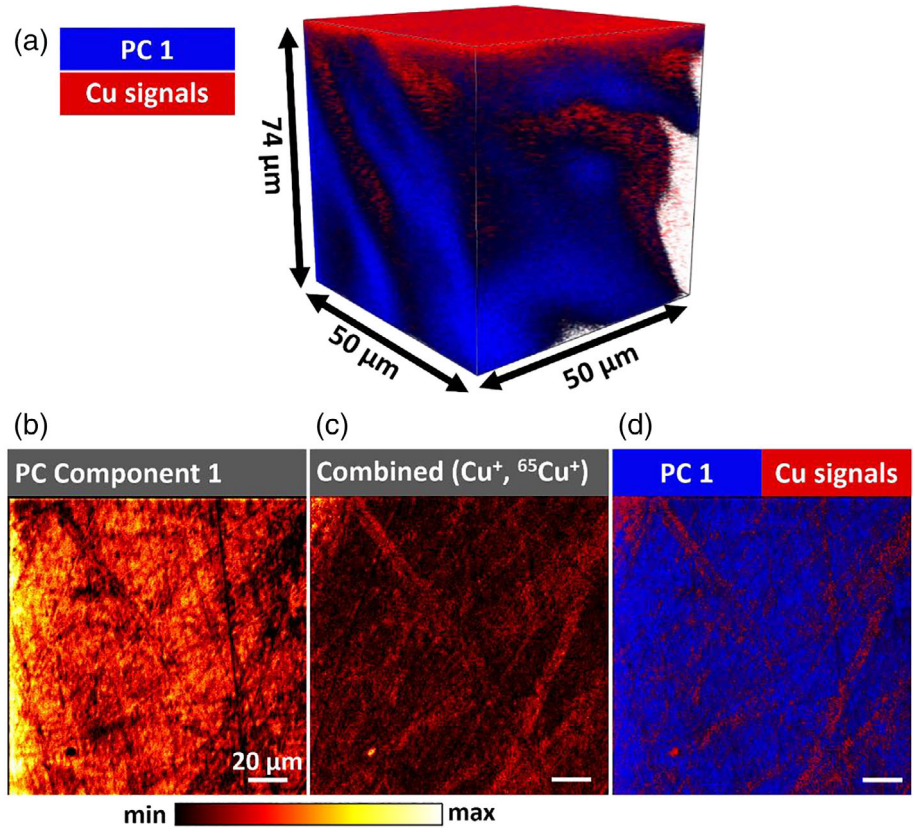

FIGURE 7 3D tomography and high-lateral-resolution imaging of Cu^{2+} diffusion. (a) 3D tomography of Cu^{2+} diffusion into polypropylene (PP). Overlay show mass fragments identified as PC component 1 in blue and Cu signals (sum of Cu^+ at m/z 62.93 and $^{65}Cu^+$ at m/z 64.92) in red. Mass fragments used for PC component 1 are: $C_3H_7^+$ at m/z 43.06, $C_4H_7^+$ at m/z 55.07, $C_4H_9^+$ at m/z 57.07, $C_5H_9^+$ at m/z 69.08, $C_5H_{11}^+$ at m/z 71.06, $C_7H_5^+$ at m/z 88.98, $C_8H_9^+$ at m/z 105.05, and $C_{11}H_{11}^+$ at m/z 143.14. Sputtering was done with a 10 keV Ar_{1500}^+ cluster beam; for analysis, Bi_3^+ primary ions were used. (b) Mass image of the sum of PP fragment ions identified as PC component 1 (Figure 3). (c) Mass image of sum of Cu^+ at m/z 62.93 and $^{65}Cu^+$ at m/z 64.92. (d) Overlay of PC 1 in blue and sum of Cu signals in red. For high-resolution imaging analysis, 25 keV Bi_3^+ primary ions were applied in delayed extraction mode [Color figure can be viewed at wileyonlinelibrary.com]

TABLE 3 Me^{2+} uptake of polypropylene (PP). PP disks were immersed each for 1 week in 10 ml of aqueous metal salt solutions. Concentrations of the solvent were determined by ICP-OES

Sample	Ni^{2+} uptake [mg (g PP)$^{-1}$]	Cu^{2+} uptake [mg (g PP)$^{-1}$]
1	103.79	18.45
2	9.76	7.23
3	9.67	16.14
4	17.47	16.14
5	10.00	14.90
Average	30.14 ± 16.52	14.57 ± 1.72

Therefore, we immersed small disks of PP for 1 week in aqueous metal salt solutions and determined the uptake from the concentration difference of the solution (beginning and end) with the help of inductively coupled plasma optical emission spectroscoopy (ICP-OES). The obtained values are given in Table 3. In average for both species significant amounts of (30.1 ± 16.5) mg Ni^{2+}/g PP and (14.6 ± 1.7) mg Cu^{2+}/g PP were obtained. The large scattering of the single values is due to the inhomogeneity of the PP samples and not an error of the ICP-OES analysis itself.

4 | DISCUSSION

The intention of this study was to investigate metal ion diffusion in commercially available PP sheets. Previous studies revealed that diffusion behavior of polymers is influenced by several factors for example, polymer morphology, polymer density, molecular weight distribution, crystallinity, glass transition temperature, or polymer melting temperature.[27,28,32–34] Here, we used an imaging mass spectrometry based method as a tool to analyze chemical metal ion diffusion in polymers.[35] Therefore a cryo-approach was established successfully to stop the diffusion process for the subsequent analysis. Imaging mass spectrometry has in comparison to other methods like permeation or weight gain the advantage that we can directly and locally resolved detect the diffusing species.

For data evaluation, we assumed a Fickian diffusion process and further on a concentration and time independent diffusion coefficient for metal ions into PP. This simple diffusion model is based on the assumption that our PP samples were homogenous and the diffusion came from an exhaustless source into semi-infinite space.[36] With this assumptions, we calculated diffusion coefficients by fitting a solution of Fick's second law of diffusion to our experimental obtained depth profile data for determination of Cu^{2+} and Ni^{2+} diffusion coefficients in dry and water-saturated PP. These mathematical fits have matched very well with our experimentally obtained data (Figures 4 and 5). The results clearly demonstrate that the assumption of Fick's diffusion is justified, and no anomalous diffusion occurs. Furthermore, we could verify with a time series that diffusion coefficient of Cu^{2+} in water-saturated PP does not vary with residence time (Table 1). This proves the validity of our general experimental approach.

Moreover, this study provides new insights into diffusion behavior of Cu^{2+} and Ni^{2+} in PP. We were able to show that diffusion coefficients of Cu^{2+} and Ni^{2+} differ (Figure 6), with Cu^{2+} ions diffusing faster into PP than Ni^{2+} ions. For Cu^{2+}, the diffusion coefficient at room temperature is $D_{PP,Cu} = (2.21 \pm 0.15)\cdot 10^{-12}$ cm^2/s, which is one order of magnitude higher compared to the diffusion coefficient of Ni^{2+} $D_{PP,Ni} = (4.43 \pm 0.55)\cdot 10^{-13}$ cm^2/s. Previous surface spectroscopy studies of polymers and metals showed that metal–polymer interaction depends on the metal reactivity. Reactive metals show stronger interactions with polymers. Thus, they diffuse slower into the polymer.[27,28] Weakly interacting metals can diffuse faster in polymers.[27] Copper is a less reactive metal compared to nickel.[27,37] Based on these previous findings, our results that diffusion of copper into PP is faster compared to diffusion of nickel can be explained and brought well in line with the literature data for different metal species.

Furthermore, the results revealed that copper and nickel ion diffusion in PP depends on the pre-treatment of the polymer. Diffusion in dry polymer was faster compared to diffusion in water-saturated polymer (Figure 6). Water sorption and diffusion in polymers is of interest in many applications, such as in drug delivery, fuel cells, and food packaging.[38] In 2000, Marais et al. investigated the permeation of water through hydrophobic and hydrophilic polymers.[36] Their study showed that water tends to build clusters in hydrophobic polyolefins. This water clustering and aggregation leads to a decrease in the diffusion coefficient. Hence, water diffusion coefficient in a water-polymer system was significantly lower than in dry polymers. It is assumed that the presence of such water clusters influences the barrier properties in polymers.[39] The formation of water clusters also depends on the polarity of the polymers.[40] The higher the hydrophobicity of the polymer matrix, the higher the formation rate of such water clusters.[38,39] We studied PP, which is a hydrophobic polymer.[36,41] The result of our experiments is consistent with the literature. The diffusion of metal ions is slower in the water-saturated polymer compared

to the dry polymer. Therefore, we assume that water clusters are formed in the water-saturated PP. These water clusters form a barrier, which slows down diffusion of the metal ions.

Another phenomenon we have detected during this study is that metal ions diffuse only into certain areas of the PP samples as it can be seen in Figures 4,5 and 7. PP is a semicrystalline polymer. In semicrystalline polymers, diffusivity depends on the size, shape and percentage of crystallites within the polymer.[42,43] Diffusion mainly occurs into amorphous regions, while crystalline regions represent obstacles and are considered impenetrable to molecules or ions.[42–44] This complicates and prolongs the diffusion path of other species into semicrystalline polymers. Based on the literature we could therefore assume that Cu^{2+} and Ni^{2+} only diffuse in amorphous areas of PP and not into the crystalline parts. Molecular structures of the outermost polymer layers determine polymer surface properties.[45,46] Surface sensible analytical methods such as ToF-SIMS and AFM, provide a full picture of the chemical composition and morphology of PP surface. AFM measurements gave us insight in PP morphology and surface roughness (Figure 1). However, we could not discriminate between crystalline and amorphous parts of PP by using AFM due to insufficient lateral resolution. ToF-SIMS imaging on the other hand revealed different surface species with the integral mass spectra fitting quite well to mass spectrometry data reported earlier.[47] Here, we demonstrated a method to image surface structure properties of semicrystalline PP. By applying PCA, we identified mass signals, which are representative for certain regions. Obviously, the fragmentation behavior of PP depends on the crystallinity. In correlation with the obtained diffusion data (Figure 7), we can state that we can differ the phases by ToF-SIMS. Phase dependent fragmentation behavior was not observed for the first time. Iuras et al used ToF-SIMS in 2016 for detecting and mapping of crystalline and amorphous surface regions in pharmaceutical materials. They correlated chemical fragments with the amorphous and crystalline surface parts of their samples.[48] Unfortunately, the direct correlation to crystallinity by high-resolution AFM failed and further experiments regarding identification of crystalline and amorphous areas of PP surface are necessary to confirm our ToF-SIMS results.

5 | CONCLUSION

In this study, we successfully applied a new ToF-SIMS cryo-approach for the determination of metal ion diffusion in PP. To the best of our knowledge, we show for the first time that cryo-ToF-SIMS can be used for analyzing metal ion diffusion into polymers. The results provide important insights regarding the diffusion properties in dry and water-saturated PP. Furthermore, this study shows that ToF-SIMS can also be used for polymer surface characterization. ToF-SIMS revealed a detailed mass spectral pattern and the mass fragments pattern are obviously correlated to the polymer structure. In summary, this method achieves satisfactory results when applied to the determination of metal ion diffusion in polymers. Therefore, in future studies, ToF-SIMS could also be applied for determination of diffusion behavior of other pollutants in various polymers. All this could be used in investigating the exposure and availability of organic contaminants and metals from polymers and microplastics. Finally, ICP-OES studies revealed that PP can take up significant, environmentally relevant, amounts of Cu^{2+} and Ni^{2+}, which are in the mg/g regime.

ACKNOWLEDGMENTS

We thank Elke Schneidenwind for her help with the ICP-OES analysis, Miguel Wiche for the AFM measurements and Sylvie Drahorad for many fruitful and stimulating discussions. M. R. especially thanks Juergen Janek, who has supported him over the years and encouraged him to enter new fields in science.

ORCID

Marcus Rohnke https://orcid.org/0000-0002-8867-950X

REFERENCES

[1] T. Rocha-Santos, A. C. Duarte, *TrAC Trends Anal. Chem.* **2015**, *65*, 47.
[2] A. L. Andrady, *Mar. Pollut. Bull.* **2017**, *119*, 12.
[3] R. Geyer, J. R. Jambeck, K. L. Law, *Sci. Adv.* **2017**, *3*, e1700782.
[4] N. B. Hartmann, T. Huffer, R. C. Thompson, M. Hassellov, A. Verschoor, A. E. Daugaard, S. Rist, T. Karlsson, N. Brennholt, M. Cole, M. P. Herrling, M. C. Hess, N. P. Ivleva, A. L. Lusher, M. Wagner, *Environ. Sci. Technol.* **2019**, *53*, 1039.
[5] PlasticsEurope Plastics—the Facts 2018, an analysis of European plastics production, demand and waste data; **2019**.
[6] S. L. Wright, R. C. Thompson, T. S. Galloway, *Environ. Pollut.* **2013**, *178*, 483.
[7] H. Jungnickel, P. Laux, A. Luch, *Toxics* **2016**, *4*, 1.
[8] H. Jungnickel, R. Pund, J. Tentschert, P. Reichardt, P. Laux, H. Harbach, A. Luch, *Sci. Total Environ.* **2016**, *563–564*, 261.
[9] A. Bakir, I. A. O'Connor, S. J. Rowland, A. J. Hendriks, R. C. Thompson, *Environ. Pollut.* **2016**, *219*, 56.
[10] L. A. Holmes, A. Turner, R. C. Thompson, *Environ. Pollut.* **2012**, *160*, 42.
[11] R. U. Halden, *Annu. Rev. Public Health* **2010**, *31*, 179.
[12] A. L. Andrady, *Mar. Pollut. Bull.* **2011**, *62*, 1596.
[13] S. H. Hong, W. J. Shim, L. Hong, *Anal. Methods* **2017**, *9*, 1361.
[14] J. H. Kwon, S. Chang, S. H. Hong, W. J. Shim, *Integr. Environ. Assess. Manag.* **2017**, *13*, 494.
[15] C. Goedecke, U. Mülow-Stollin, S. Hering, J. Richter, C. Piechott, A. Paul, U. Braun, *J. Environ. Anal. Chem.* **2017**, *4*, 1.

[16] B. C. I. Chinyere, O. N. Kieran, *Eur. J. Biomed. Pharm. Sci.* **2018**, *5*, 124.
[17] E. Davarpanah, L. Guilhermino, *Estuarine, Coastal Shelf Sci.* **2015**, *167*, 269.
[18] M. Vincent, P. Hartemann, M. Engels-Deutsch, *Int. J. Hyg. Environ. Health* **2016**, *219*, 585.
[19] K. K. Das, R. C. Reddy, I. B. Bagoji, S. Das, S. Bagali, L. Mullur, J. P. Khodnapur, M. S. Biradar, *J. Basic Clin. Physiol. Pharmacol.* **2018**, *30*, 141.
[20] Q. Han, Y. Huo, L. Yang, X. Yang, Y. He, J. Wu, *Molecules* **2018**, *23*, 1.
[21] S. Naderi-Gohar, K. M. Huang, Y. Wu, W. M. Lau, H. Y. Nie, *Rapid Commun. Mass Spectrom.* **2017**, *31*, 381.
[22] D. Nečas, P. Klapetek, *Open Phys.* **2012**, *10*, 181.
[23] M. Jablonska, S. Reissaus, S. Henning, M. Menzel, A. Hahnel, J. Klehm, U. Hirsch, A. Heilmann, *Micron* **2019**, *124*, 102685.
[24] M. E. Kroeger, B. A. Sorenson, J. S. Thomas, E. A. Stojkovic, S. Tsonchev, K. T. Nicholson, *J. Vis. Exp.* **2014**, *92*, e52164.
[25] J. P. Hofmann, M. Rohnke, B. M. Weckhuysen, *Phys. Chem. Chem. Phys.* **2014**, *16*, 5465.
[26] M. Karimi, Diffusion in polymer solids and solutions. in *Mass Transfer in Chemical Engineering Processes* (Ed: D. J. Marko), InTechOpen, Rijeka, Croatia **2011**.
[27] F. Faupel, R. Willecke, A. Thran, *Mater. Sci. Eng.* **1998**, *R22*, 1.
[28] F. Faupel, V. Zaporojtchenko, Metal diffusion in polymers and on polymer surfaces. in *Diffusion Processes in Advanced Technological Materials* (Ed: D. Gupta), Springer, Berlin, Heidelberg **2005**.
[29] J. Crank, *The mathematics of diffusion*, 2nd ed., Oxford University Press, Ely House, London W.I **1975**.
[30] L. H. Sperling, *Introduction to Physical Polymer Science*, 4th ed., Wiley-Interscience, USA **2006**.
[31] C. Kern, M. Quade, S. Ray, J. Thomas, M. Schumacher, T. Gemming, M. Gelinsky, V. Alt, M. Rohnke, *J. R. Soc. Interface* **2019**, *16*, 20180638.
[32] A. Reynier, P. Dole, S. Humbel, A. Feigenbaum, *J. Appl. Polym. Sci.* **2001**, *82*, 2422.
[33] W. Limm, H. C. Hollifield, *Food Addit. Contam.* **1996**, *13*, 949.
[34] R. M. Town, H. P. van Leeuwen, R. Blust, *Front. Chem.* **2018**, *6*, 627.
[35] S. J. Miklavcic, M. Nydén, J. B. Lindén, J. Schulz, *RSC Adv.* **2014**, *4*, 60349.
[36] S. Marais, Q. T. Nguyen, C. Devallencourt, M. Metayer, T. U. Nguyen, P. Schaetzel, *J. Polym. Sci. B Polym. Phys.* **2000**, *38*, 1998.
[37] W. F. Kieffer, *J. Chem. Educ.* **1950**, *27*, 659.
[38] E. M. Davis, Y. A. Elabd, *J. Phys. Chem. B* **2013**, *117*, 10629.
[39] A. Du, D. Koo, G. Theryo, M. A. Hillmyer, R. A. Cairncross, *J. Membr. Sci.* **2012**, *396*, 50.
[40] H. W. Starkweather, *J. Polym. Sci.C Polym. Lett.* **1963**, *1*, 133.
[41] D. Bochicchio, E. Panizon, L. Monticelli, G. Rossi, *Sci. Rep.* **2017**, *7*, 6357.
[42] M. Hedenqvist, U. W. Gedde, *Prog. Polym. Sci.* **1996**, *21*, 299.
[43] F. Nilsson, M. S. Hedenqvist, U. W. Gedde, *Macromol. Symp.* **2010**, *298*, 108.
[44] F.-M. Preda, A. Alegría, A. Bocahut, L.-A. Fillot, D. R. Long, P. Sotta, *Macromolecules* **2015**, *48*, 5730.
[45] C. M. Chan, L.-T. Weng, *Materials* **2016**, *9*, 1.
[46] C.-M. Chan, L.-T. Weng, Y.-T. R. Lau, *Rev. Anal. Chem.* **2014**, *33*, 11.
[47] S. Kern, C. Kern, M. Rohnke, *Surf. Sci. Spectra* **2019**, *26*, 025003.
[48] A. Iuras, D. J. Scurr, C. Boissier, M. L. Nicholas, C. J. Roberts, M. R. Alexander, *Anal. Chem.* **2016**, *88*, 3481.

SUPPORTING INFORMATION

Additional supporting information may be found online in the Supporting Information section at the end of this article.

How to cite this article: Kern S, Kern C, Pradja MM, Düring R-A, Rohnke M. Spatially resolved indiffusion behavior of Cu^{2+} and Ni^{2+} in polypropylene. *J Appl Polym Sci*. 2021;138:e49655. https://doi.org/10.1002/app.49655